AD-A083 778 ROCKWELL INTERNATIONAL THOUSAND OAKS CA ELECTRONICS--ETC F/6 7/4
HIGH RESISTIVITY MOLECULAR BEAM EPITAXIAL ALGAAS FOR DEVICE APP--ETC(U)
FEB 80 R D FAIRMAN, D L MILLER, W A HILL N00014-78-C-0370
UNCLASSIFIED ERC41006.2AR NL

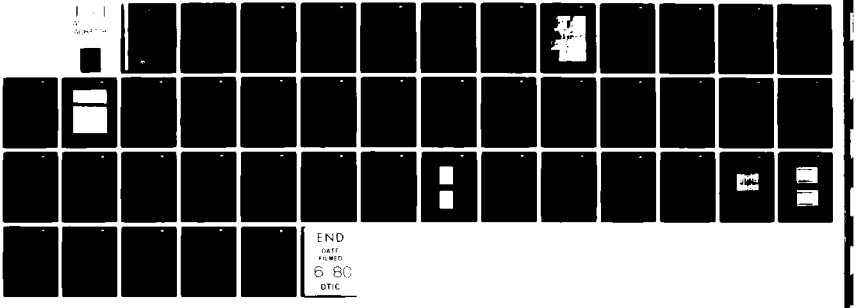

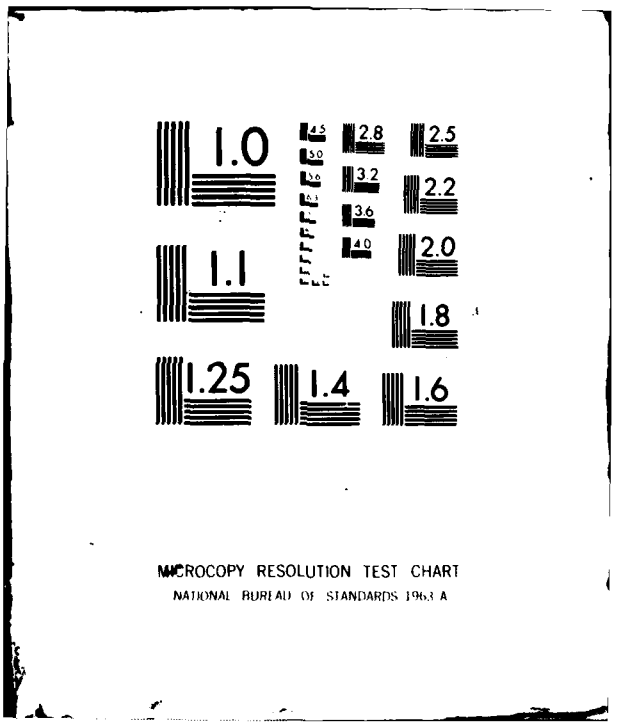
1.0
1.1
1.25
1.4
1.6
1.8
2.0
2.2
2.5
2.8
3.2
3.6
4.0
MICROCOPY RESOLUTION TEST CHART
NATIONAL BUREAU OF STANDARDS 1963 A

LEVEL II

ERC41006.2AR

Copy No. 18

HIGH RESISTIVITY MOLECULAR BEAM EPITAXIAL AlGaAs FOR DEVICE APPLICATIONS

ANNUAL REPORT FOR THE PERIOD
May 1, 1978 through April 30, 1979

GENERAL ORDER NO. 41006
CONTRACT NO. N00014-78-C-0370

DOCUMENT NO. ERC41006.2AR

Prepared for

Office of Naval Research
800 North Quincy Street
Arlington, VA 22217

D. R. Ch'en
Principal Investigator

FEBRUARY 1980

Rockwell International

Unclassified

SECURITY CLASSIFICATION OF THIS PAGE (When Data Entered)

REPORT DOCUMENTATION PAGE

READ INSTRUCTIONS BEFORE COMPLETING FORM

1. REPORT NUMBER: ERC41006.2AR
2. GOVT ACCESSION NO.: AD-A083 778
3. RECIPIENT'S CATALOG NUMBER:

4. TITLE (and Subtitle): (6) High Resistivity Molecular Beam Epitaxial AlGaAs for Device Applications
5. TYPE OF REPORT & PERIOD COVERED: 5/01/78 thru 4/30/79
6. PERFORMING ORG. REPORT NUMBER: (14) ERC41006.2AR

7. AUTHOR(s): (10) R. D. Fairman, D. L. Miller, W. A. Hill
8. CONTRACT OR GRANT NUMBER(s): (15) N00014-78-C-0370

9. PERFORMING ORGANIZATION NAME AND ADDRESS:
Rockwell International
Electronics Research Center
1049 Camino Dos Rios, Thousand Oaks, Ca. 91360

10. PROGRAM ELEMENT, PROJECT, TASK AREA & WORK UNIT NUMBERS:
PE62762N
RF-581-001
NR 251-032
(12) 45

11. CONTROLLING OFFICE NAME AND ADDRESS:
Office of Naval Research
800 North Quincy Street
Arlington, Virginia 22217
411391

12. REPORT DATE: 2/1980
13. NUMBER OF PAGES: 41

14. MONITORING AGENCY NAME & ADDRESS (if different from Controlling Office):
See Block 11
(16) F581000

15. SECURITY CLASS. (of this report): Unclassified
15a. DECLASSIFICATION/DOWNGRADING SCHEDULE:

16. DISTRIBUTION STATEMENT (of this Report):
Approved for public release. Distribution unlimited.
(11) Feb 80
(17) RF581001

17. DISTRIBUTION STATEMENT (of the abstract entered in Block 20, if different from Report):
(9) Annual Rept. 1 May 78-30 Apr 79

18. SUPPLEMENTARY NOTES:
ONR Scientific Officer
Telephone: (202) 696-4218

19. KEY WORDS (Continue on reverse side if necessary and identify by block number):
Molecular beam epitaxy (MBE), Aluminum gallium arsenide (AlGaAs), GaAs field-effect transistor (GaAs FET).

20. ABSTRACT (Continue on reverse side if necessary and identify by block number):
AlGaAs & GaAs molecular beam epitaxial (MBE) layers suitable for device application, are studied and the results are discussed. Analysis includes Van der Pauw and Hall measurements, photoluminescence, sheet resistance, photo-induced current transient spectroscopy (PITS), secondary ion spectroscopy, and capacitance-voltage profiling. All indications are that high quality buffer layers of AlGaAs and active layers of GaAs can be produced by MBE which can yield devices of exceptional performance.

DD FORM 1 JAN 73 1473 EDITION OF 1 NOV 65 IS OBSOLETE

Unclassified

SECURITY CLASSIFICATION OF THIS PAGE (When Data Entered)

411391

TABLE OF CONTENTS

		Page
1.0	INTRODUCTION	1
2.0	TECHNICAL DISCUSSION	3
2.1	Molecular Beam Growth Technology	3
2.2	MBE AlGaAs Buffer - Active Layer Growth	6
2.2.1	Growth of Undoped AlGaAs	6
2.2.2	Growth of AlGaAs:H_2	9
2.2.3	Growth of AlGaAs:O_2	11
2.2.4	Growth of GaAs(Ge)/AlGaAs FET Structures	12
3.0	MATERIAL CHARACTERIZATION	13
3.1	Van der Pauw Measurements	13
3.2	Capacitance-Voltage Profiling	14
3.3	Photoluminescence Measurements	16
3.4	Photo-induced Transient Current Measurements	17
3.5	Secondary Ion Mass Spectrometry	22
3.6	Sheet Resistance Measurements	25
3.7	Transistor Test Structures	29
4.0	SUMMARY	32
4.1	SIMS Profiles of GaAs/AlGaAs Structures	32
4.2	PITS Measurements of MBE GaAs/AlGaAs Layers	32
4.3	H_2 and O_2 Doping Experiments	32
4.4	Evaluation of GaAs/AlGaAs Structures	33
5.0	TRANSISTOR RESULTS	34
5.1	Device Fabrication	34
5.2	Device Characterization	34
6.0	CONCLUSION	37
7.0	FUTURE PLANS	38
8.0	REFERENCES	39

LIST OF FIGURES

		Page
Fig. 2.1	Molecular Beam Epitaxy Laboratory	4
Fig. 2.2	Mobility of MBE GaAs	5
Fig. 2.3	SEM micrograph of AlGaAs epilayer on GaAs	10
Fig. 3.1	Impurity concentration profile of MBE n-GaAs/AlGaAs	15
Fig. 3.2	Photoluminescence measurement of semi-insulating MBE AlGaAs at 77°K	18
Fig. 3.3	Thermally stimulated current and photo-induced current transient spectroscopy scans of MBE AlGaAs	19
Fig. 3.4	Experimental setup of PITS measurement apparatus	21
Fig. 3.5	Typical synchronous PITS waveforms	23
Fig. 3.6	PITS spectra for two MBE AlGaAs samples	24
Fig. 3.7	SIMS profile of AlGaAs/GaAs	26
Fig. 3.8	SIMS profile of oxygen doped AlGaAs/GaAs	27
Fig. 3.9	SIMS profile of oxygen implanted GaAs	28
Fig. 3.10	I-V characteristics of high resistivity AlGaAs	30
Fig. 5.1	FET devices fabricated from MBE slices 170 and 210	35
Fig. 5.2	FET I-V characteristics of MBE slices 170 and 210	36

1.0 INTRODUCTION

The advancement of III-V MESFET technology requires, in part, the improvement of semi-insulating materials used in today's device fabrication. The properties of currently available chromium-doped GaAs substrates impose restrictions on the performance of devices and monolithic circuits presently being produced in research laboratories. Therefore, new high performance materials will be an essential part of future device development. Already, successful growth of lattice matched, semi-insulating, wide bandgap AlGaAs layers on GaAs has been achieved and therefore this technique offers a very attractive avenue to impact advanced device development.

The effort in this program is to investigate the growth of high resistivity AlGaAs by molecular beam epitaxy, with the goal of developing a heterostructure insulating layer technology with current confinement properties for microwave GaAs FETs. It is our intention to exploit the attractive features of MBE for producing high quality material for microwave devices. The key features and results of our program begin with the investigation of AlGaAs epitaxy from advanced MBE growth techniques. This has led to the successful growth of AlGaAs films with sheet resistivities of 10^9 Ω/□ to 10^{10} Ω/□. Films have also been grown over a range of 0 to 30 atomic percent Al, all with excellent semi-insulating properties.

Improvements in the design and construction of metal sources in the basic MBE apparatus have resulted in a reduction of acceptor impurities and an overall improvement in low temperature Hall mobility. Several techniques have been used to characterize AlGaAs properties. Basic determinations of impurity concentration in AlGaAs by the use of Van der Pauw and C-V measurements have been inconclusive, although preliminary results obtained by photo-induced transient current (PITS) measurements suggest a continuum of deep levels throughout the bandgap. Other techniques used for characterization have been photoluminescence and secondary ion mass spectrometry (SIMS). These have proven to be useful in defining some of the details in the nature of the new insulating films. Further efforts to identify principal levels and capture cross sections will be required.

The overall assessment of this new technology is in the performance of microwave devices. Epitaxial structures of GaAs(Ge) on AlGaAs have been used for the fabrication of 1 μm gate length low noise FETs and preliminary dc transistor characteristics have been obtained.

This report describes our research activity in detail. Section 2.0 is a technical discussion of the MBE effort on this program. Included is both GaAs and AlGaAs layer growths. Section 3.0 presents the methods and results of our material characterization activities, Section 4.0 is a summary of these results. Section 5.0 discusses the results obtained on device structures fabricated from MBE material. Our conclusions are discussed in Section 6.0 with a presentation of future plans in Section 7.0.

2.0 TECHNICAL DISCUSSION

2.1 Molecular Beam Growth Technology

In molecular beam epitaxy, growth of GaAs is achieved by the simultaneous deposition of Ga and As onto a heated GaAs substrate. The details of this technique have been discussed extensively in the literature and will not be presented here, except to discuss those points which are specifically relevant for the production of AlGaAs/GaAs structures. The Molecular Beam Epitaxy Laboratory is shown in Fig. 2.1 illustrating two MBE reactors that were designed and fabricated at Rockwell Electronics Research Center, Thousand Oaks, California.

Success in producing an AlGaAs buffer FET structure depends on the ability to grow high resistivity, semi-insulating AlGaAs; to grow high mobility GaAs epilayers of controlled thickness and appropriate doping profile; and to achieve an abrupt transition between AlGaAs and GaAs without a significant number of interface states. Growth of n-type GaAs with mobilities sufficient for FET production is now relatively routine. Figure 2.2 shows mobility at 77°K and 300°K as a function of carrier density for n-type GaAs grown by MBE at the Electronics Research Center, Thousand Oaks. A calculated theoretical maximum is also indicated.

From a materials standpoint, the two major areas of development in this project are (1) the growth of suitable AlGaAs, and (2) the growth and characterization of a suitable GaAs-AlGaAs interface. In the first task, growth of AlGaAs with a low density of electrically active, unintentional impurities is an initial step. Once this is achieved, the addition of selected impurities can pin the Fermi level at the desired position to give semi-insulating material. For the second task, the growth parameters which influence the number and type of interface states must be investigated. Additionally, the communication of the deep levels added intentionally to the AlGaAs (to make it semi-insulating) with the GaAs active region must be investigated, and may determine which impurities are suitable for AlGaAs design. Finally, the doping profile in the GaAs active layer must be appropriate for an FET device.

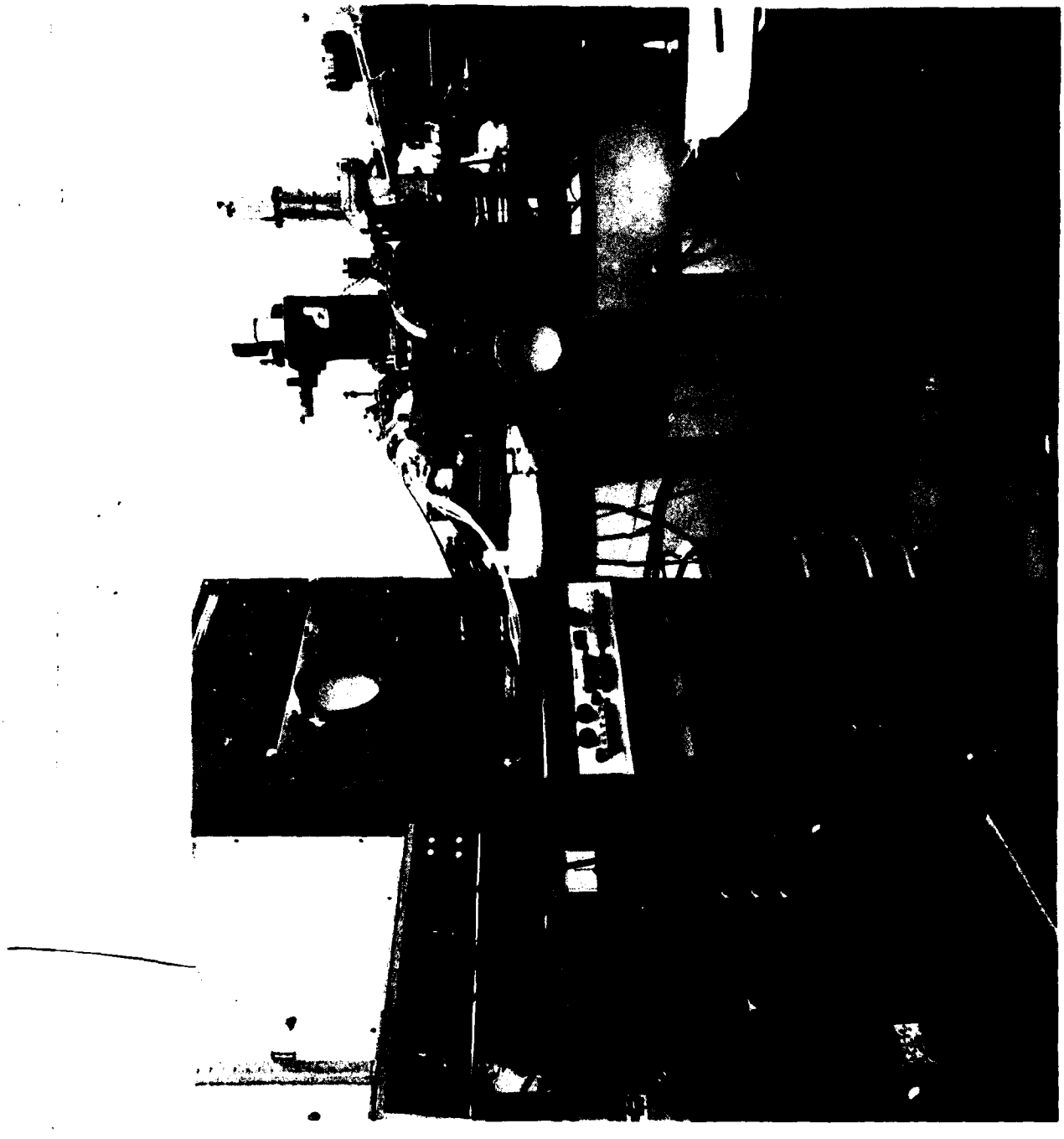

Fig. 2.1 Molecular beam epitaxy laboratory.

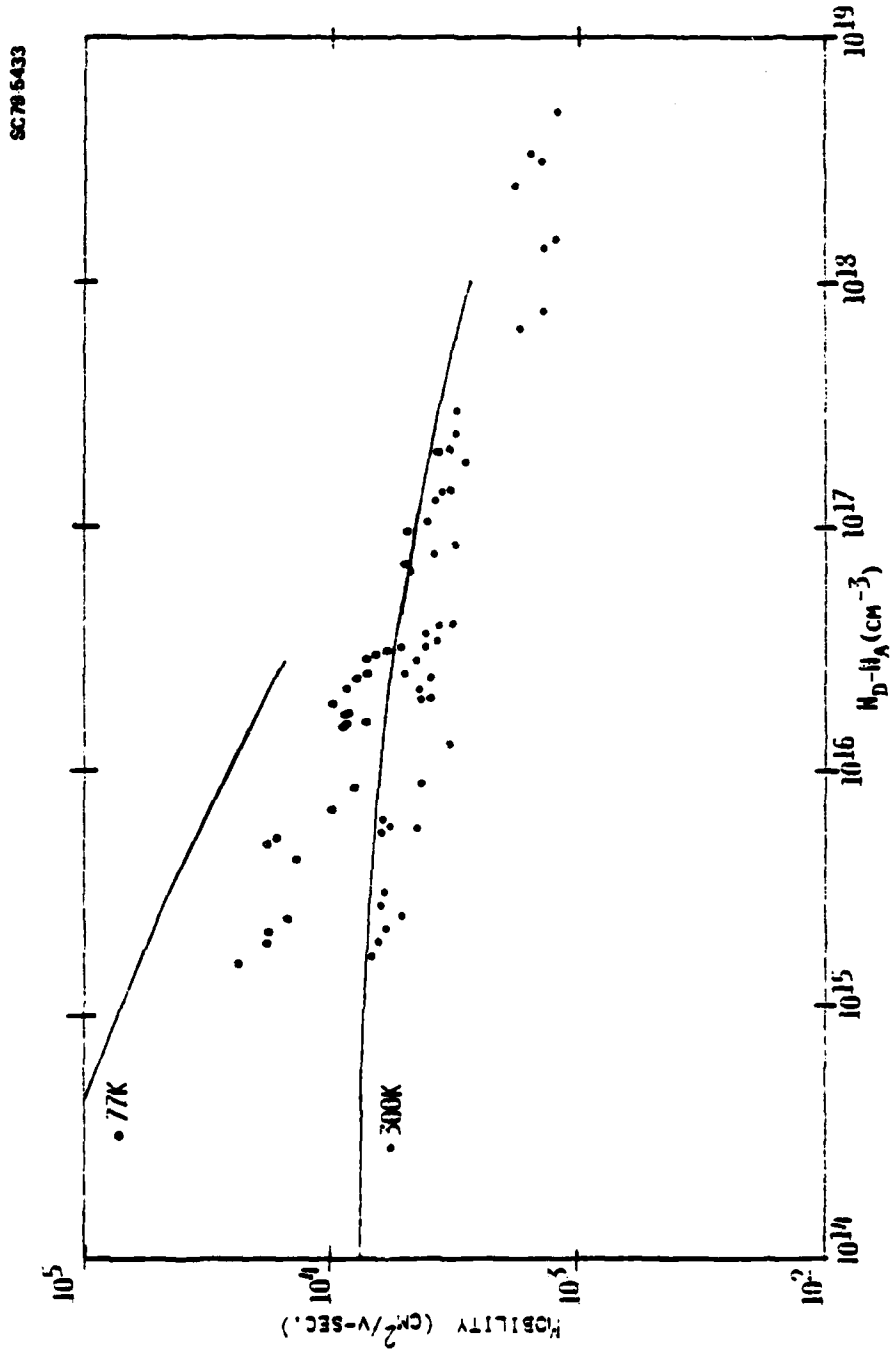

Fig. 2.2 Mobility of MBE GaAs.

There are several important parameters involved in the growth of suitable semi-insulating AlGaAs. These all involve the control of unintentional electrically active impurities or defects in the AlGaAs layers. These can arise from background gasses in the vacuum chamber during layer growth, from impurities in the starting materials, or from growth conditions which lead to large numbers of vacancies or interstitials. The reactive nature of Al makes it extremely important to achieve a very low background pressure during deposition. Our chamber is equipped with an airlock for substrate insertion, and extensive liquid nitrogen shrouding, which keep O_2 and H_2O levels below 1×10^{-11} torr. The major source of background gas contamination is CO, produced in the Ga and Al sources, which has a partial pressure of $\sim 5 \times 10^{-10}$ torr during layer growth. This low pressure has been achieved during the past year by, among other things, installing a 10°K closed cycle helium refrigerator cryogenic pump, which pumps CO much more efficiently than the ion pump on the chamber. Other design modifications of sources and shrouding have also served to decrease the level of background gasses in the chamber. These are discussed in more detail in the next section.

2.2 MBE AlGaAs Buffer - Active Layer Growth

A list of layers grown by MBE for this project is shown in Table 2.1. Several configurations were attempted, with two different dopants used for the GaAs active layer, and three different growth conditions for the AlGaAs buffer layer. These conditions and the materials behind their growth is presented here.

2.2.1 Growth of Undoped AlGaAs

Residual gasses in the vacuum chamber affect the properties of AlGaAs grown by MBE. In particular, gasses containing oxygen such as H_2O, CO, or CO_2 can lead to oxygen incorporation and deep electronic levels in the material. In order that the number and type of unintentional deep levels is kept relatively small, steps have been taken to reduce unintentional oxygen

Table 2.1

Layers Grown for MBE AlGaAs Buffer FET Program

Date	Growth #	Purpose	Comments
5/10	262	GaAs(Sn)/AlGaAs(0) graded junction	
5/9	261	GaAs(Sn)/AlGaAs(0) abrupt junction	
4/25	247	AlGaAs calibration (with 5204)	
~4/20		SnTe source	System contamination
4/5	241	GaAs/AlAs/AlGaAs/ GaAs(n-Sn)/GaAs(n^+Sn)	AlAs wrinkled after oxidation in air
2/19	213	GaAs(Ge)/AlGaAs(0)	
2/19	212	GaAs(Ge)/AlGaAs(0) calibration	
2/16	211	GaAs(Ge)/AlGaAs(H_2)	
2/16	210	GaAs(Ge)/AlGaAs(H_2) calibration	
2/15	209	GaAs(Ge)/AlGaAs undoped	
2/15	208	GaAs(Ge)/AlGaAs undoped calibration	
2/14	207	n-type AlGaAs w/H_2 (shared growth)	
~1/23	New source constructed tested		
1/23/79	203	GaAs(Ge)/AlGaAs(0)	
1/19/79	202	GaAs(Ge)/AlGaAs(0)	
1/18/79	201	GaAs(Ge)/AlGaAs(0)	
2/11/79	195	AlGaAs	

Table 2.1 (Cont'd)

Date	Growth #	Purpose	Comments
11/17/78	173	GaAs(Sn)/AlGaAs(0)	$n = 6 \times 10^{16}$ cm^{-3}
11/15/78	171	GaAs(Ge)/AlGaAs(0)	$n = 5 \times 10^{17}$ cm^{-3}
11/14/78	170	GaAs(Ge)/AlGaAs(0)	$n = 2 \times 10^{17}$ cm^{-3}
11/10/78	169	GaAs(Ge)/AlGaAs(0)	$n = 5 \times 10^{17}$ cm^{-3}
11/10/78	168	GaAs(Ge)/AlGaAs(0)	2000A/10^{17} depleted
9/6/78	139	AlGaAs calibration	
9/5/78	138	AlGaAs calibration	
9/1/78	137	AlGaAs calibration	
6/16/79	113	AlGaAs calibration	
6/15/79	112	AlGaAs calibration	
6/13/78	111	GaAs (undoped)	GaAs background doping
6/9/78	110	GaAs (undoped) 3.6 μm	
6/6/78	108	GaAs (undoped) 4 μm	
6/2/78	106	GaAs (undoped)	

incorporation in the AlGaAs layers. This was undertaken primarily with other funding and funding partly provided by another ONR project (Contract No. N00014-78-C-0330). These steps consisted of providing additional pumping, cryogenic shielding, and reducing degassing from the Al and Ga sources. These details are discussed in the final report for that contract. The result was a considerable improvement in deep level concentration of the $Al_xGa_{1-x}As$, as determined by donor activation and luminescence efficiency. The activation of Sn donors was found to depend on the growth parameters, down to below $n = 1 \times 10^{16}$ cm^{-3} at $x = 0.3$. This suggests that interactions of donors with native defects, probably gallium vacancies, dominates the donor activation, as has been recently reported.[1] If this model is applicable, then the deep level concentration due to unintentional impurity incorporation would be below about 5×10^{16} cm^{-3} in our best material. The undoped AlGaAs was semi-insulating ($R_s > 10^9$ Ω/□) and was used for several FET layer growths. A scanning electron micrograph of an AlGaAs epilayer on GaAs is shown in Fig. 2.3. Here the epilayer is about 1.5 μm thick.

2.2.2 Growth of AlGaAs with H_2

Since it was reported[2] that introduction of H_2 into an MBE chamber during growth of GaAs has resulted in a decrease in layer electrical compensation and an increase in electron mobility, AlGaAs was grown in a hydrogen atmosphere. H_2 filtered through an Ag/Pd alloy diffusion element was introduced into the growth chamber through a variable leak valve. This also resulted in semi-insulating material, and studies performed on n-type AlGaAs showed that H_2 incorporation did not result in any observed reduction in deep level density. At the time these experiments were done, however, the deep level density was large (>10^{18} cm^{-3}), so that smaller reductions would not have been observed. A considerable increase in H_2O partial pressure was observed following the introduction of H_2 into the chamber. The time constant of the H_2O signal suggested this was caused by a reaction of H_2 with oxides in the chamber, rather than oxygen contamination in the H_2 gas inlet. Therefore, growth in an H_2 background was not continued at this time.

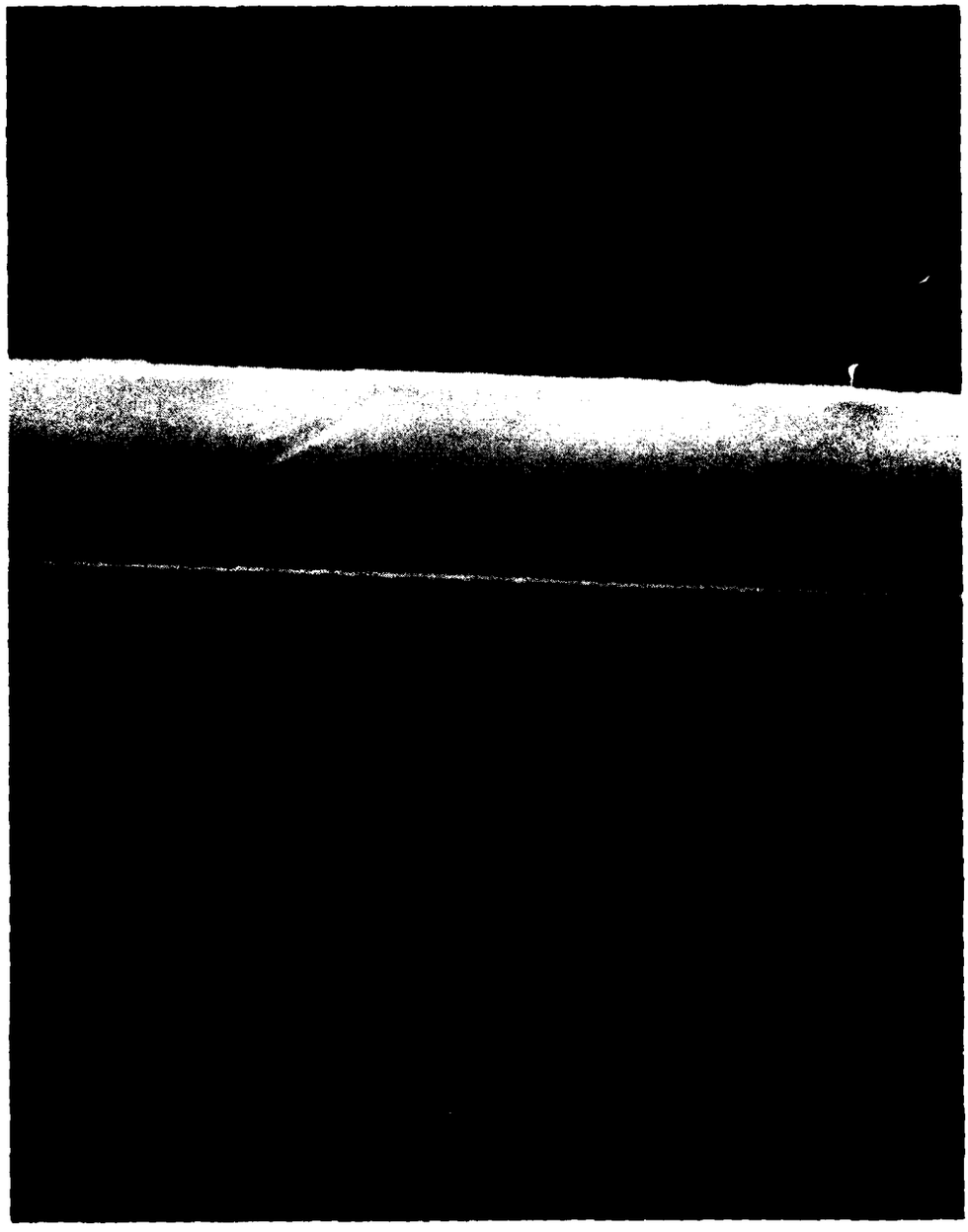

Fig. 2.3 SEM micrograph of AlGaAs epilayer on GaAs.

2.2.3 Growth of AlGaAs with O_2

There have been a number of reports in the literature of semi-insulating AlGaAs produced by MBE growth in an O_2 atmosphere.[3] This is the approach we have chosen for producing semi-insulating AlGaAs buffer layers. The oxygen is incorporated much more heavily in AlGaAs than in GaAs, presumably due to the reactive nature of Al.

The $Al_xGa_{1-x}As$ buffer layers have been grown 1-2 μm thick in oxygen partial pressures of 5×10^{-7} torr to 1×10^{-6} torr, with x = .3 to .4, and at a growth rate of 1-1.5 μm/hr. The oxygen was obtained from a one liter glass flask, and was bled into the system through a bakable variable leak valve. The chamber ion pump was turned off during the AlGaAs(O) growth, and pressure maintained by balancing the oxygen leak rate with the O_2 pumping speed of the 10K cryogenic sorption pump. This constant throughput mode of operation provides continuous pumping of the chamber during the layer growth, with continuous removal of gasses such as CO or CO_2.

The AlGaAs layer appearance and microscopic defect density is unaffected by O_2 pressures in this range, and GaAs layers grown over them appear comparable to layers grown directly on GaAs substrates. A SIMS profile of Al, As, and Cr content was performed* for one O-doped and one undoped GaAs/AlGaAs buffer structure. Interfaces on both layer growths were abrupt, although about .01% Al was detected in the GaAs grown over the undoped layer, while .1% was detected in the GaAs grown over the oxygen-doped layer. This is compared to a detection limit of .005% for Al for the two measurements. It is not known whether this effect is real or an artifact of the measurement technique. Chromium was also observed at a level about one order of magnitude below the substrate concentration in the GaAs grown on the undoped buffer layer, and a factor of 5 below the substrate level for GaAs grown on O-doped AlGaAs. More SIMS profiling will be necessary to investigate the extent of Cr and Al diffusion into the active layer.

* by C. A. Evans & Associates
1670 S. Amphlett Blvd.
Suite 120
San Mateo, CA 94402

2.2.4 Growth of GaAs/AlGaAs FET Structures

Growth of the GaAs active layer on the AlGaAs buffer layers has proceeded by valving off whatever gas was being admitted (H_2 or O_2), closing the Al shutter, and opening the dopant shutter. The ion pump was then started so removal of O_2 from the system was very rapid; pressures of less than 10^{-10} torr oxygen were achieved in several minutes. H_2 pumping was somewhat slower.

Two different dopants have been used in making FET structures. These are Ge and Sn. Sn gives better GaAs mobilities, but does not readily give abrupt doping profiles. This is due to Sn surface segregation during growth of the layer. Abrupt profiles can be achieved with Ge, but great care must be taken with the substrate temperature and As/Ga flux ratios to obtain good mobilities with this amphoteric dopant. Most of the layers were grown using Ge as the dopant.

A source of SnTe was also constructed and put in the growth chamber following reports of good mobilities with abrupt doping profiles from this compound.[4] The source was degassed, but never used, since background doping levels increased from about $n = 2 \times 10^{15}$ cm^{-3} to $n = 2 \times 10^{17}$ cm^{-3} coincident with the introduction of this source. It is suspected that this was due to Te_2 contamination of the growth chamber, although there was no conclusive evidence of Te_2 incorporation in the layers. This background doping persisted for over two months, despite the immediate removal of the SnTe source, and despite a number of attempts to reduce the background level by cleaning the chamber parts and replacing the source.

3.0 MATERIAL CHARACTERIZATION

GaAs and $Al_xGa_{1-x}As$ layers grown in this program have been examined with the following measurement techniques:

1. Van der Pauw (ρ, μ_H, N_D-N_A at 300, 77°K)
2. Photoluminescence, 77°K
3. Sheet resistance, 300°K
4. Photo-induced transient current
5. Secondary ion mass spectroscopy
6. Capacitance voltage profiling

3.1 Van der Pauw Measurements

Early in the program efforts were made to evaluate the background impurity level of the MBE system. Several samples were produced with epitaxial layers in the thickness range of 1-4 μm. Van der Pauw measurements of these undoped MBE GaAs are shown in Table 3.1. Net donor density observed during this period was in 1-2 × 10^{15} cm^{-3} range and electron mobilities of 6450 cm^2-V^{-1}-sec^{-1} at 300°K and 18,100 cm^2-V^{-1}-sec^{-1} at 77°K were obtained. Net doping density observed for these samples by C-V profiling indicated higher doping than by Van der Pauw measurement.

Epitaxial films grown on Cr compensated substrates usually show a dead layer effect due to anomalies caused by either chromium migration or interface states. Films grown by vapor and liquid phase epitaxy have shown these effects and FETs fabricated from such layers produce backside gating effects. Recent work by Charles Evans and Associates with SIMS analysis have shown effects of Cr migration on all growths of epitaxial films produced on Cr compensated substrates.[5] Diffusion rates of Cr have been indicated. These analytical results correlate with the need to grow thick layer structures for measurement of carrier densities <10^{14} cm^{-3}.

Table 3.1
UNDOPED MBE GaAs

CV Measurement (300°K)			Hall Measurement (300/77°K)	
Sample	N_d-N_a (cm^{-3})	t (μm)	N_d-N_a (cm^{-3})	μ_H (cm^2-V^{-1}-sec^{-1})
106	8.2×10^{15}	1.7	$11.0\text{-}9.6 \times 10^{15}$	3438-9968
108	4.0×10^{15}	2.8	$4.8\text{-}3.6 \times 10^{15}$	3203-7074
111	3.2×10^{15}	2.3	$4.0\text{-}3.2 \times 10^{15}$	3108-8952
114	4.0×10^{15}	1.7	$2.0\text{-}1.9 \times 10^{15}$	6450-18,100

$Al_xGa_{1-x}As$ layers grown in this program have not been measured by Van der Pauw due to the high resistance properties of the as-grown layers. Sheet conductance effects with the semi-insulating GaAs substrate make mobility measurements meaningless. All AlGaAs layers prepared in this program have shown extremely high resistance properties.

3.2 Capacitance-Voltage Measurements

Depletion capacitance profiling was performed using evaporated aluminum Schottky barriers. A large area forward biased contact was used to contact the surface of layers grown on semi-insulating substrates or AlGaAs buffer layers. A Materials Development Corp. profiling system was used to make the measurement which utilized a 1 MHz Booton capacitance meter.

Capacitance voltage profiling was performed on undoped MBE GaAs layers and on intentionally doped GaAs grown in-situ upon AlGaAs buffers. Capacitance measurements made upon AlGaAs buffers show extremely low capacitance per unit area in the range of 500 pF cm^{-2}. Negatively biased Schottky barriers exhibited no signs of further depletion as the built-in voltage had already depleted the structure. Trap density measurements of AlGaAs layers will be approximated using photo-induced current spectroscopy. Heavily doped GaAs active layers grown in situ upon AlGaAs buffer layers were profiled and produced well-behaved doping profiles with abrupt interfaces as shown in Fig. 3.1.

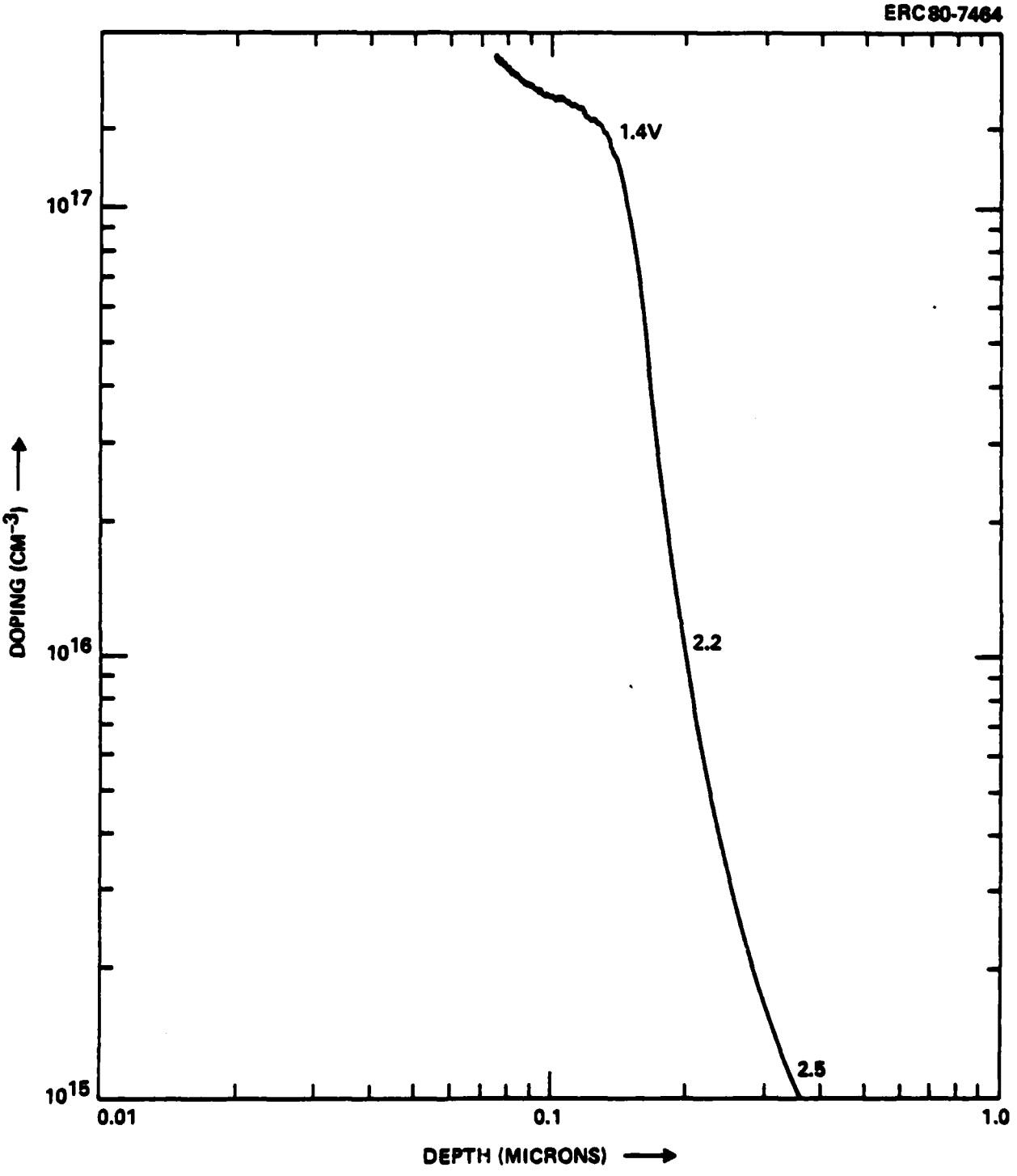

Fig. 3.1 Impurity concentration profile of MBE n-GaAs/AlGaAs.

3.3 Photoluminescence Measurements

Photoluminescence measurements were made on $Al_xGa_{1-x}As$ at 77°K to determine the alloy composition, for $x < 0.35$. The aluminum fraction x was determined from the relation:

$$x = (9569\text{Å})/\lambda(77°K) - 1.163 \quad (1)$$

Equation (1) was obtained from published values of the composition dependent bandgap, the temperature dependent GaAs bandgap and the composition dependent difference in photoluminescence peaks between 77°K and 300°K, i e.,

$$Eg(x,77°K) - Eg(x\ 300°K) \equiv \Delta Eg(x). \quad (2)$$

The composition dependent energy gap was taken to be[6]

$$Eg(x,300°K) = 1.424\ eV + 1.247x\ eV. \quad (3)$$

The difference between 300°K and 77°K photoluminescence peak positions as a function of composition has been reported as[7]

$$\Delta Eg(x) = \Delta Eg(0)\ [1 + 0.6x]\ . \quad (4)$$

The value of $\Delta Eg(0)$ can be obtained from[8]

$$Eg(0,T) = 1.519\ eV - (5.405\times10^{-4}T^2)(T + 204)^{-1}\ eV \quad (5)$$

Combining Eq. (2) through (6) gives

$$Eg(x,77°K) = 1.509\ eV + 1.298x\ eV. \quad (6)$$

Converting to wavelength and solving for x gives Eq. 1. For heavy O_2-doped $Al_xGa_{1-x}As$, luminescent efficiency was too low to allow this type of measurement. Values of x were estimated from Al source temperature in these cases. A typical semi-insulating $Al_xGa_{1-x}As$ photoluminescence spectrum taken at 77°K is shown in Fig. 3.2.

3.4 Photo-induced Transient Current Measurements

The quality of substrate and of epilayer material and the response of this material to process variables is crucial to device performance. Further improvements in device performance are, therefore, tied to improvements in semi-insulating buffer layer and process control. To this end we have developed a photo-induced transient spectroscopy technique (PITS) for the examination of bulk and surface impurity and defect states in the band gap of semi-insulating materials.

A variety of experimental tools have been used in the study of trapping phenomena in semiconductors and insulators, including thermally stimulated current (TSC), deep level transient spectroscopy (DLTS), photocapacitance/conductance and photoluminescence. Until recently only TSC has been an effective transport measurement for the study of insulating and semi-insulating materials, since capacitance methods such as DLTS require either a Schottky barrier or p-n junction, and are largely ineffective in the presence of a high series resistance. However, in the past year a new photo-induced current transient spectroscopy (PITS) method has been developed at the Rockwell International Electronics Research Center[9] and elsewhere[10] which shows great potential as a highly sensitive tool for the study of impurity and defect trapping levels in insulating or semi-insulating materials (Fig. 3.3). This technique has been referred to as optical - DLTS, although we prefer the nomenclature PITS since the technique involves the observation of photocurrent transients rather than capacitance transients in a depletion region. It is similar to DLTS measurements in that the magnitude and time constant of observed phototransients are proportional to the concentration and emission rate of trapping levels in the material.[11] Like TSC measurements, however, the PITS technique can be used with either ohmic or Schottky barrier contacts and on insulating or semi-insulating materials. Other features of the PITS method are:

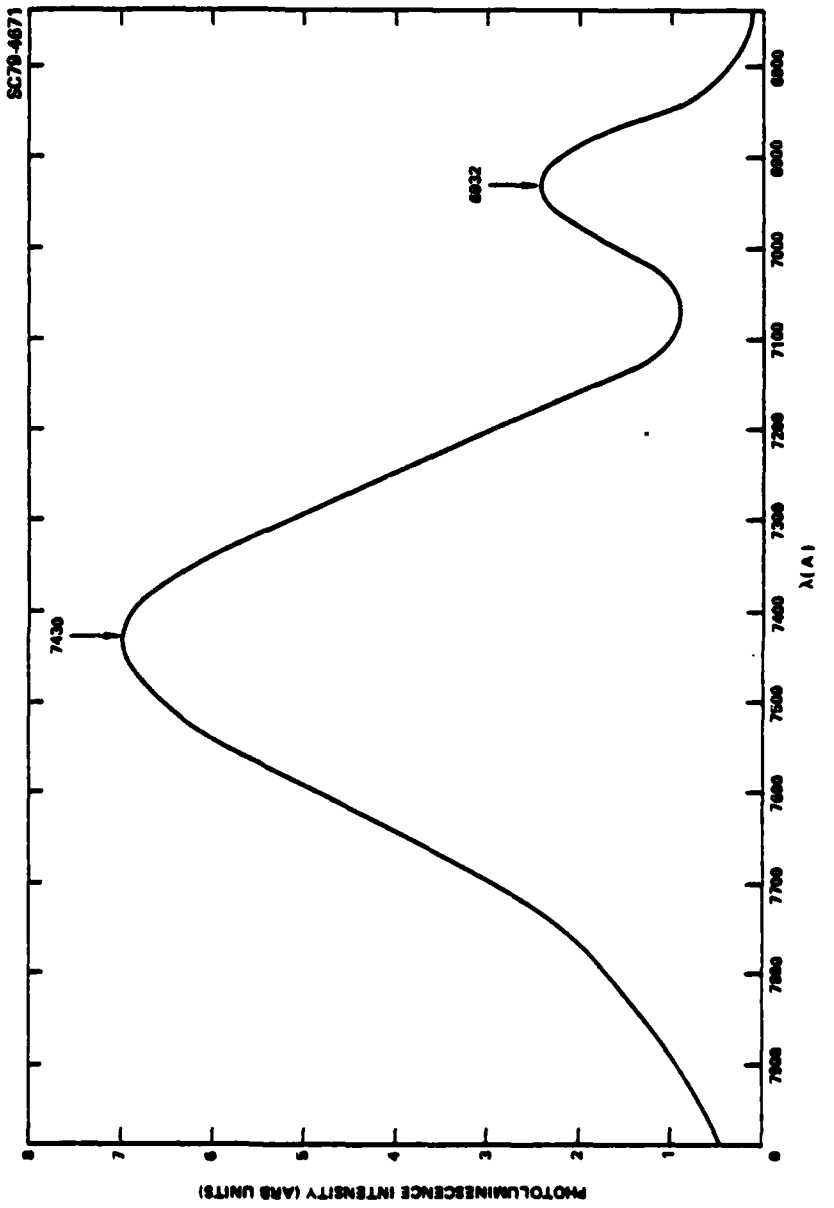

Fig. 3.2 Photoluminescence measurement of semi-insulating MBE AlGaAs at 77°K.

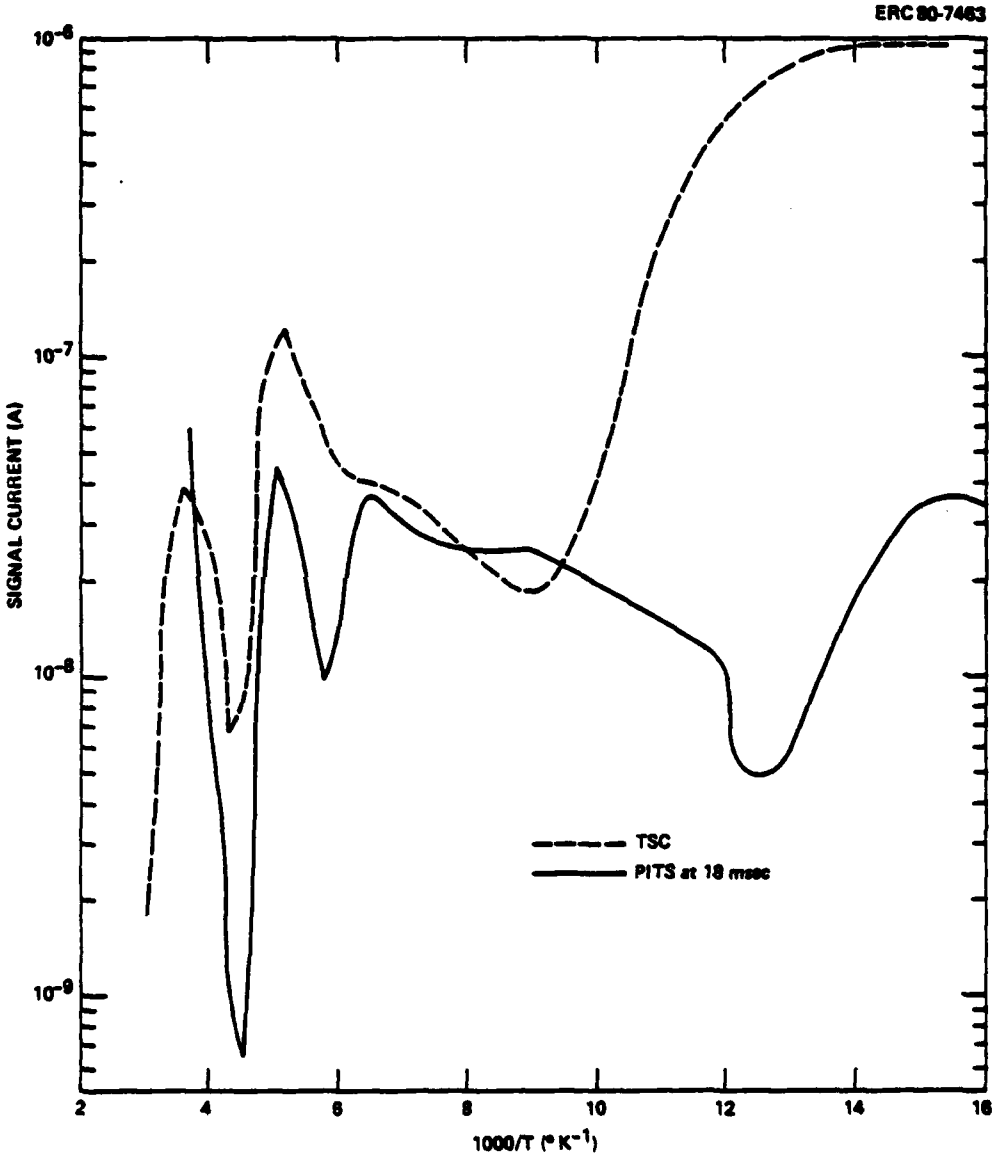

Fig. 3.3 Thermally stimulated current and photo-induced current transient spectroscopy scans of MBE AlGaAs.

(1) It is a spectroscopic tool, in that it provides information on trap concentration, emission rate, and energy.
(2) It is high in sensitivity.
(3) It is potentially able to examine all traps from the band edge to mid-gap.
(4) It can detect traps even in the presence of high dark (equilibrium) conductivity.
(5) It can differentiate between bulk and surface effects through variation of the illumination wavelength.
(6) It detects both trap filling and emptying processes.

Experimental Technique

PITS is a transport technique which detects the transient rise or decay of the sample photocurrent during chopped illumination. A typical PITS spectrum is obtained by sampling either the photo current rise (R-PITS) or decay (D-PITS) at two points in time, with the current difference $\Delta I = [I(t_1) - I(t_2)]$ recorded continuously as a function of temperature. Any peaks observed in the spectrum will correspond to a trap emission rate e_t which is directly proportional to the sampling rate $\Delta t^{-1} = (t_2 - t_1)^{-1}$. Successive temperature scans at different sampling rates can therefore determine both the trap energy and capture cross section, assuming a single-exponential rise or decay.

A block diagram of the apparatus used at the Electronics Research Center is shown in Fig. 3.4. The sample is maintained under a constant dc bias while illuminated with chopped monochromatic light. The resulting photocurrent is detected by a high-speed pre-amplifier (PARC 181). The output of the pre-amplifier is fed to a sample/hold amplifier followed by a lock-in detector. The sampling points t_1, t_2 are determined by sample gate pulses generated by the chopper reference signal, f, and the internally-generated 2f signal of the lock-in.

The method of detection used here is equivalent to the DLTS method using a double-boxcar integrator. The sampling time constant Δt is varied by

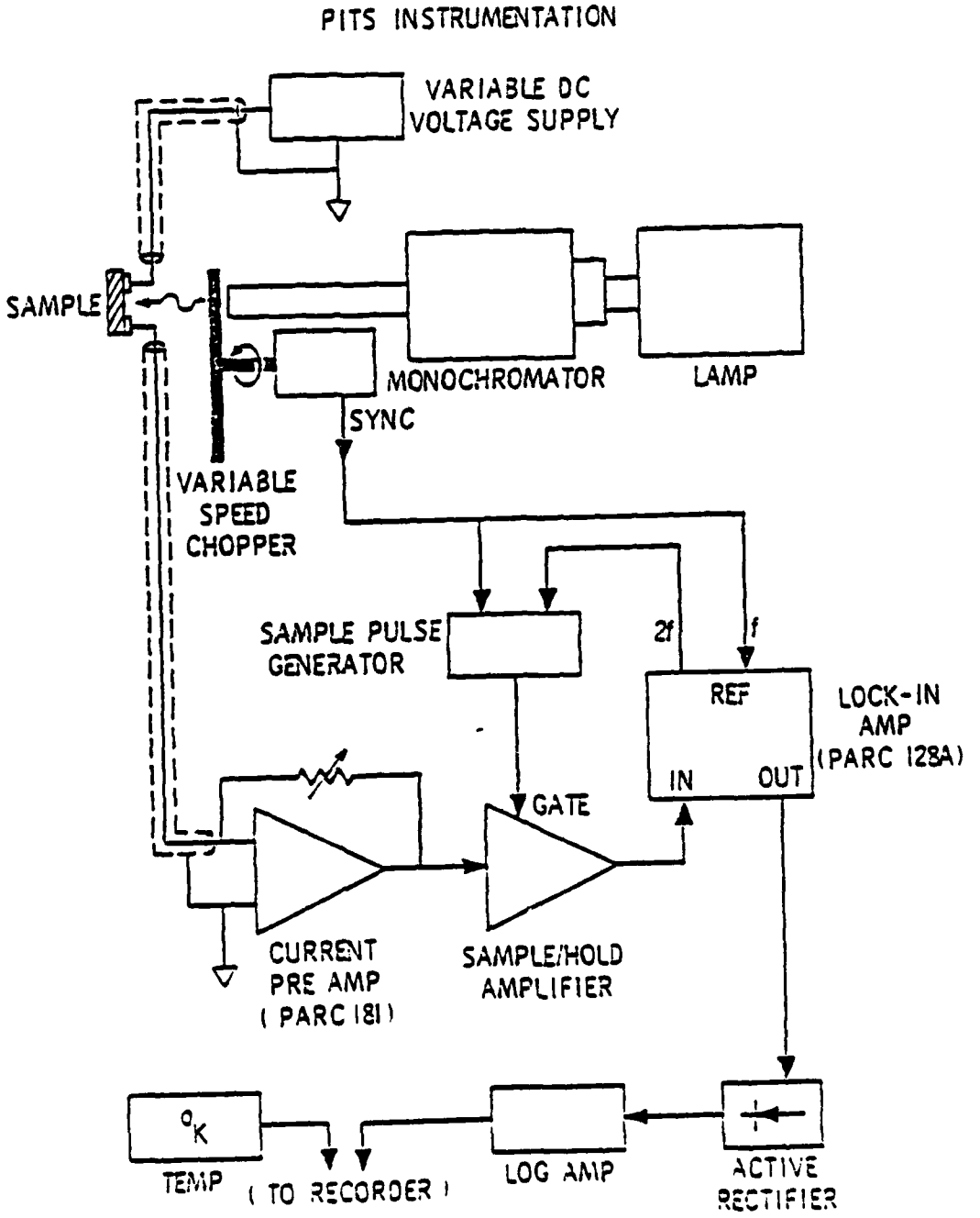

Fig. 3.4 Experimental setup of PITS measurement apparatus.

changing the chopping rate; the present apparatus has a range of 0.37 to 18 msec. The sample temperature can be varied from 60°K to 500°K; thus, all except very shallow traps (<0.1 eV) can be observed. Surface and epilayer measurements are made using closely spaced (5-15 μm) ohmic surface contacts and slightly greater than bandgap illumination. Substrate measurements are made using an additional ohmic base contact and slightly less than bandgap light to insure reasonably uniform illumination throughout the bulk. DC bias voltages are maintained at moderate levels in order to prevent any high-field current injection. The ability of PITS to differentiate between the surface and substrate of a given sample without additional processing steps (e.g., sequential etching) has proven to be a unique and highly useful property of the technique.

The magnitude of a particular PITS peak is a function of the trap emission rate and the degree of trap filling. Under the simplified assumptions of complete trap filling and a single time constant exponential decay, the magnitude of the free carrier concentration is given by

$$\Delta n(t) = N_t e_t \tau \exp[-e_t t]$$

where N is the trap concentration and τ is the free-carrier lifetime. A typical waveform using chopped illumination is shown in Fig. 3.5. In some instances, however, a transient signal "inversion" can take place; this corresponds to a transient overshoot in the case of R-PITS and undershoot for D-PITS, as shown in Fig. 3.5(b). Such an "inversion" is possible in the case of a shallow trap and a deep recombination center where the trap cross section S_t is much smaller than the recombination center cross section S_r.[12] PITS spectra for AlGaAs samples grown in this program are shown in Fig. 3.6.

3.5 Secondary Ion Mass Spectroscopy

SIMS is an especially sensitive tool for determining low impurity concentration profiles in semiconductor materials. AlGaAs and GaAs/AlGaAs interfaces have been analyzed by this technique. Recent reports of Cr-

(a) TRAP DECAY: $\Delta n \cong N_t e_t \tau \exp\left[-e_t t\right]$

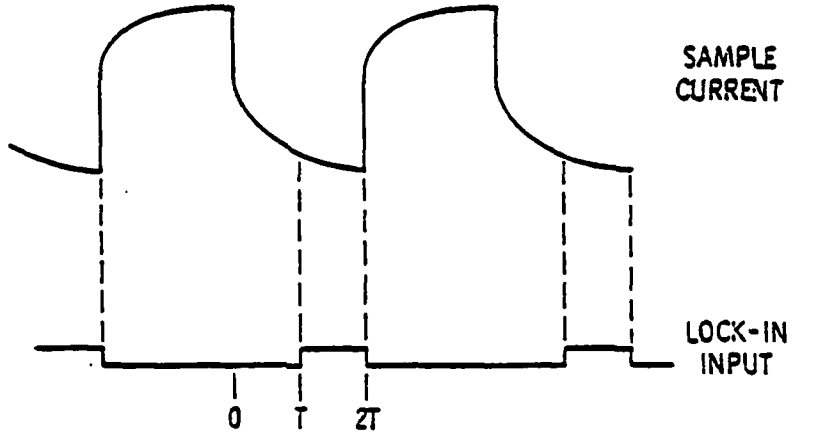

(b) SIGNAL INVERSION (OVERSHOOT/UNDERSHOOT)

$$\frac{S_t}{S_r} < \exp\left[\frac{E_T - E_{FO}}{kT}\right]$$

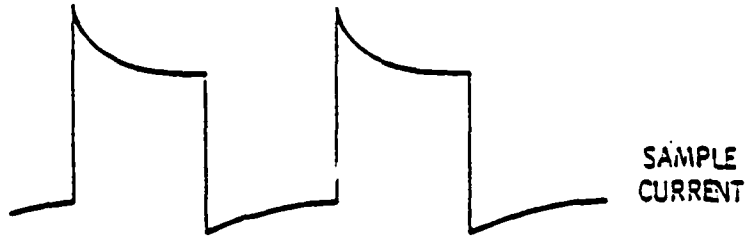

Fig. 3.5 Typical synchronous PITS waveforms.

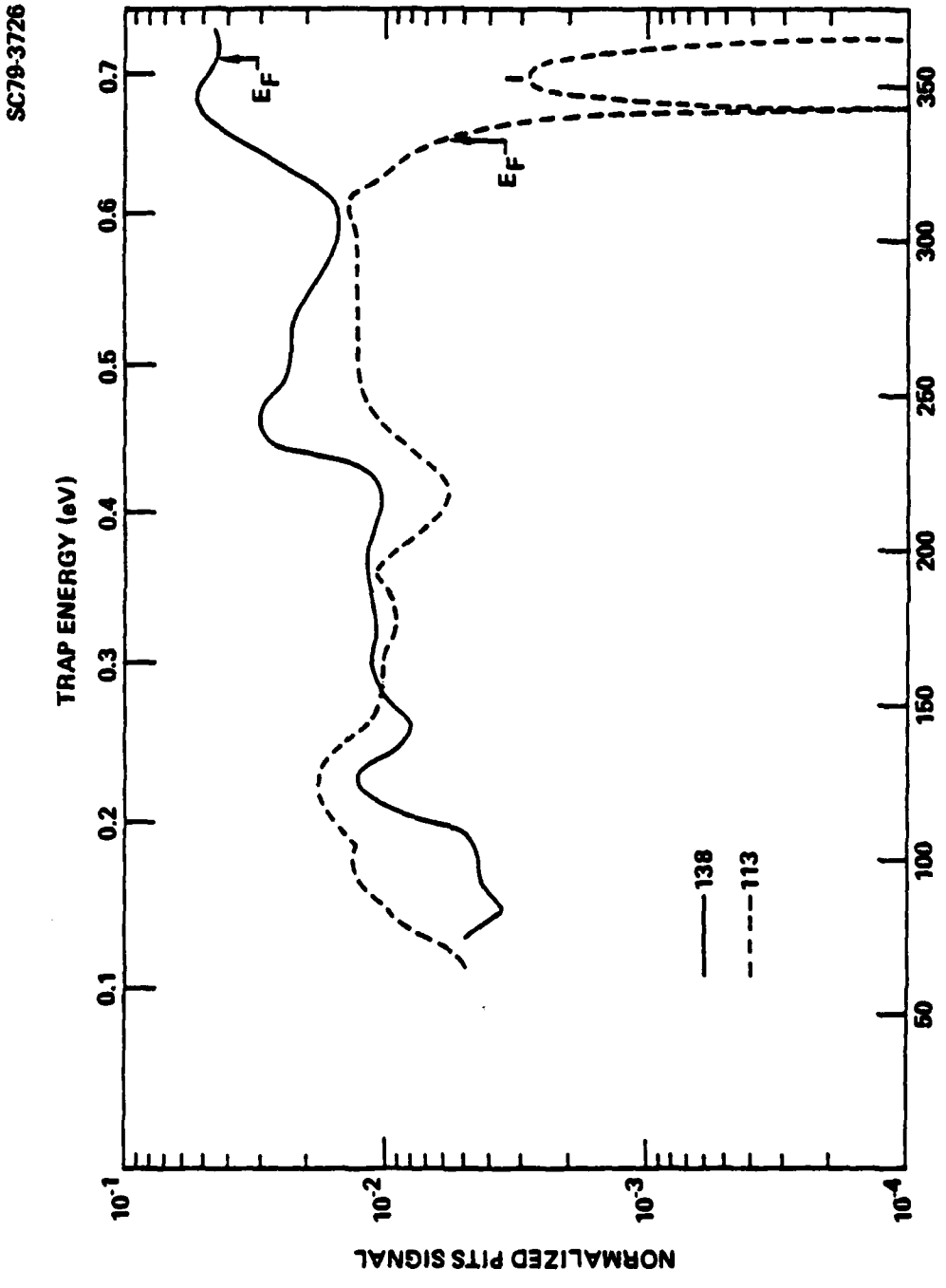

Fig. 3.6 PITS spectra for two MBE AlGaAs samples.

redistribution have shown sensitivity for Cr down to low 10^{15} cm^{-3} concentrations in GaAs. Evidence of the abrupt nature of the AlGaAs/GaAs structure and the control of various constituents during epitaxial growth is shown in Fig. 3.7. Figure 3.8 shows another SIMS profile of an identical structure in which the AlGaAs was O_2 doped. In both samples the interface between GaAs and AlGaAs is abrupt with respect to Al. (The transition at the interface is less than 250A.) Chromium appears to exhibit slightly greater outdiffusion in the O_2 doped sample. The change in Cr signal at each interface is an artifact of the specific sputtering rates of GaAs and AlGaAs in O_2.

Samples of undoped and O_2 doped AlGaAs were sent to Cornell University and to Charles Evans and Associates for O_2 analysis by SIMS. Analysis standards were prepared by implanting O_2 into epitaxial GaAs with 100 KeV, 1.90×10^{12} cm^{-2} dose. Analysis of the O_2 implanted and as-grown samples can be run in the same system evacuation to normalize the background effects. Initial results from SIMS analysis of the O_2 implanted samples gave reasonable profiles as in Fig. 3.9. This related well to the O_2 distribution expected. Subsequent measurement of both standard and MBE samples were not reproducible due to high background levels in the SIMS apparatus. Replacing the sputtering beam with a cesium beam increased sensitivity but the background level of 10^5 counts/sec was still much too high to detect O_2 concentrations at less than 10^{16} cm^{-3}. Back sputtering effects and the reactive nature of the samples prevented a more sensitive analysis. Additional efforts are in progress to replace the ion pumps with cryogenic pumps in order to reduce the background level of O_2 in the chamber.

3.6 Sheet Resistance Measurements

Measurement of sheet resistance has become an important characterization method for high resistivity materials and has been used extensively for semi-insulating GaAs bulk and epitaxial layer evaluation. Numerous sample geometries have been used; a standard Van der Pauw pattern and FET device patterns utilizing source and drain contacts are used routinely. Minimal contact resistance is important in assessing the absolute value of the sheet resistance measurement. Using our standard evaporated and alloyed Au-Ge/Pt contact

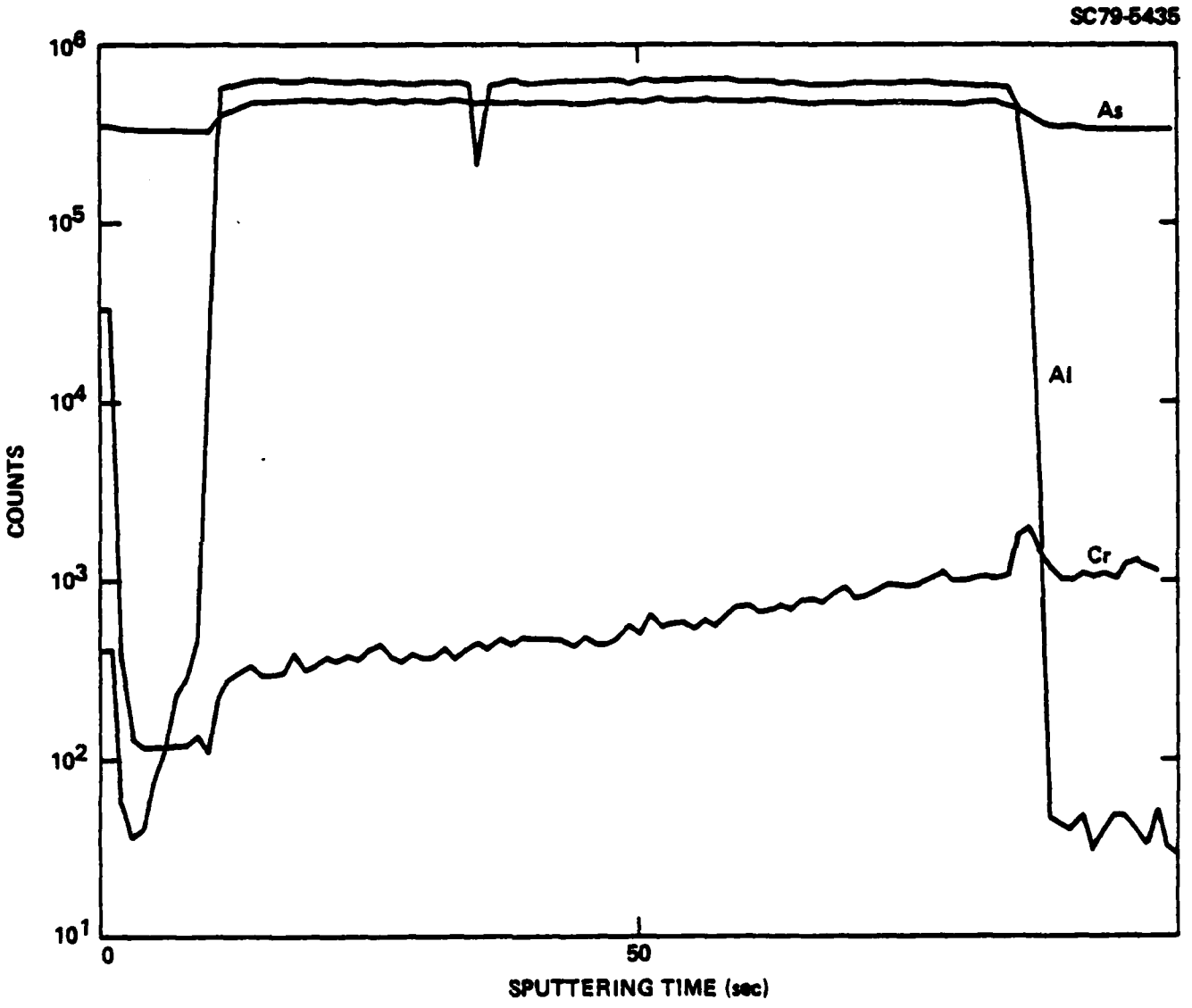

Fig. 3.7 SIMS profile of AlGaAs/GaAs.

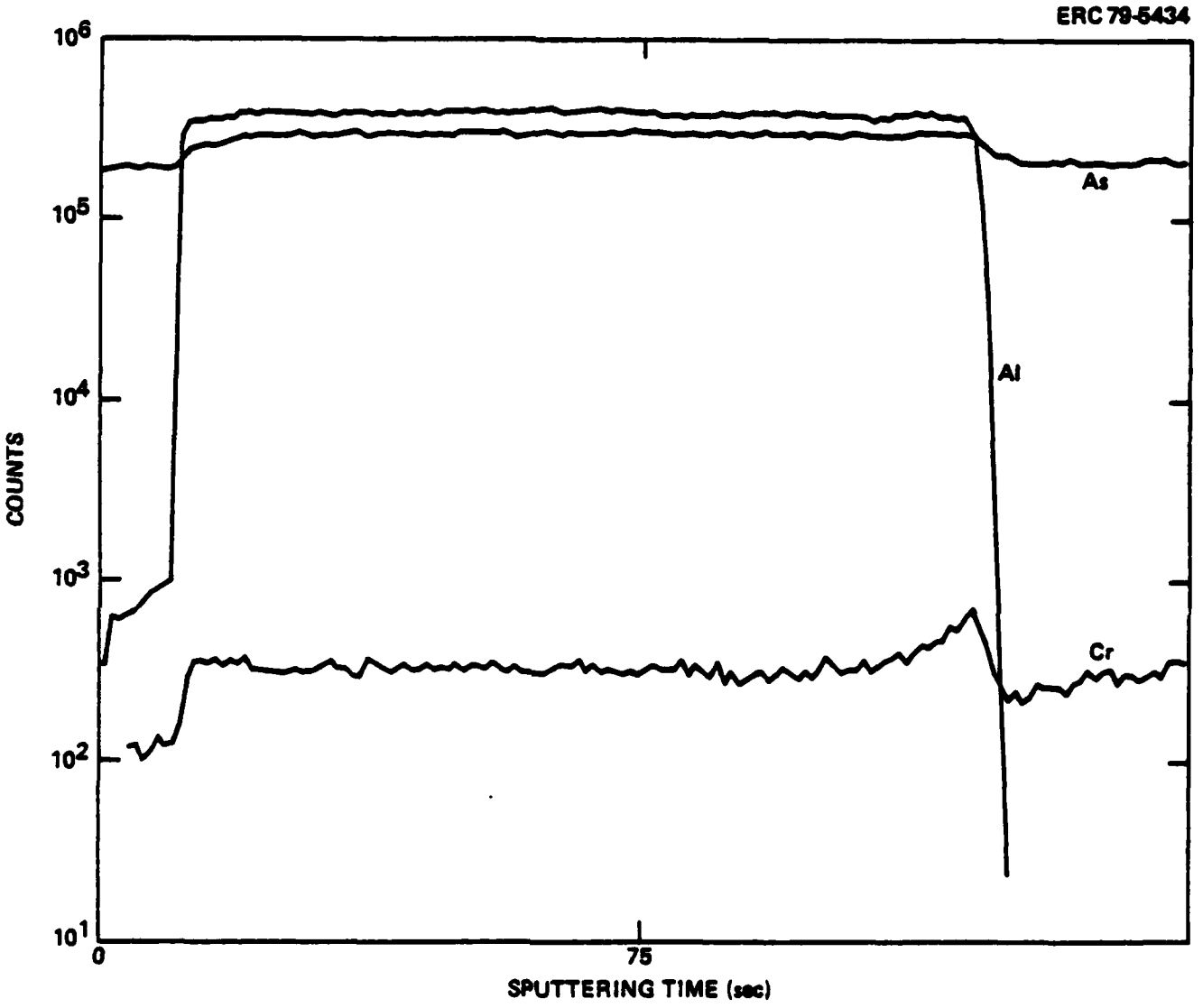

Fig. 3.8 SIMS profile of oxygen doped AlGaAs/GaAs.

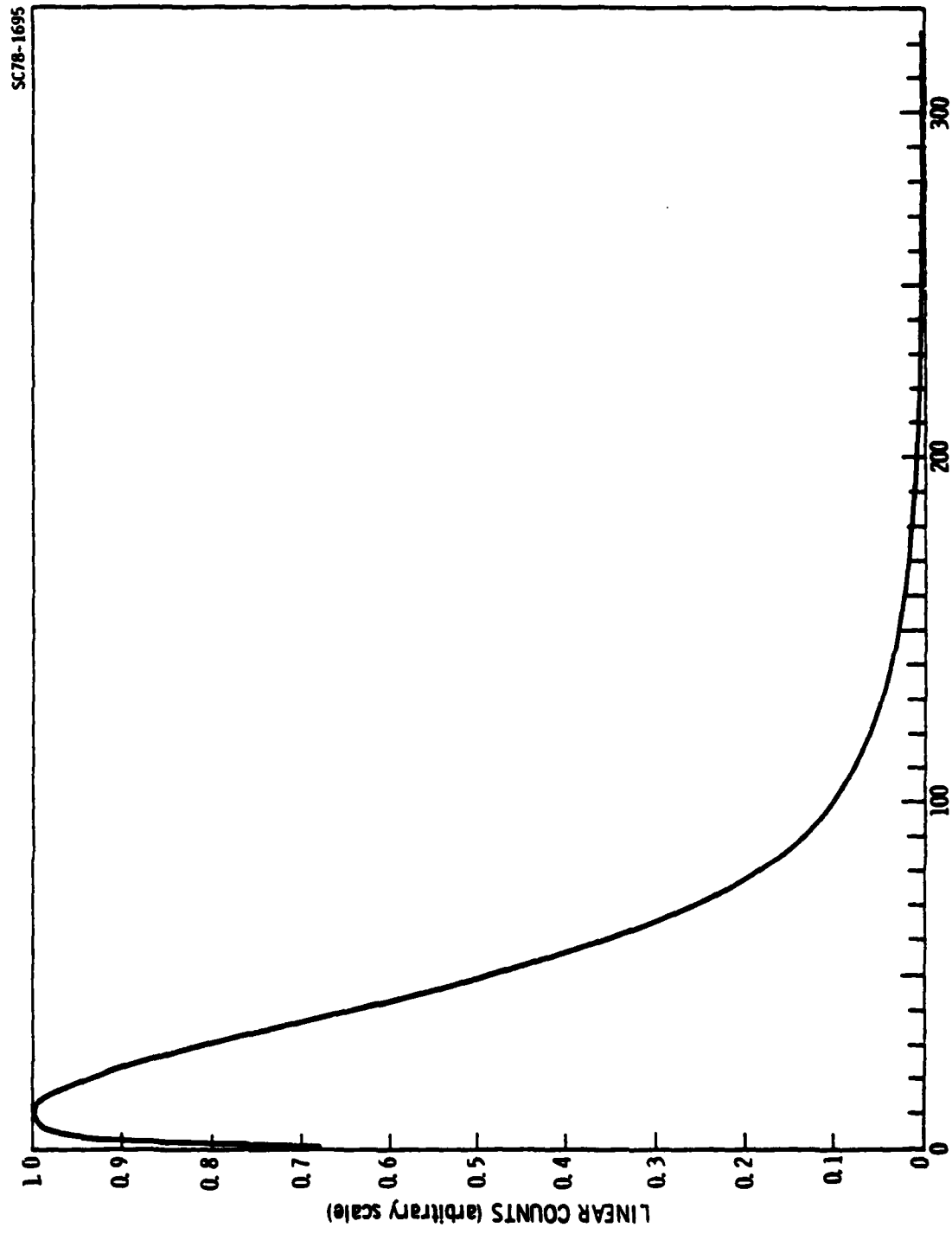

Fig. 3.9 SIMS profile of oxygen implanted GaAs.

on device material, we normally measure a specific contact resistance of ~1 × 10^{-6} Ω-cm^2. Use of this contact with Cr doped or undoped semi-insulating GaAs has been highly successful. Comparison measurements of this with Au-Ge/Pt contacts made on localized n^+ implants into semi-insulating GaAs showed no change in the resultant sheet resistance of a high resistivity sample. Figure 3.10 shows the I-V characteristic of two AlGaAs samples used for sheet resistance measurements. The resistance is taken at a bias voltage of 50-100 V. Measurement of sheet resistance under ambient light conditions produced less reproducible results with higher resultant sheet resistance values than measurements taken in the dark. Table 3.2 shows sheet resistance values from a series of MBE AlGaAs layers grown in this program.

Table 3.2

Sheet Resistance Measurements

Sample No.	Sheet Resistance (Ω/□)	Comments
113	5.0 × 10^9	Undoped AlGaAs
137	1.7 × 10^{10}	Undoped AlGaAs
138	6.7 × 10^{10}	Undoped AlGaAs
169	5.0 × 10^{10}	O_2 doped AlGaAs
170	2.5 × 10^{10}	O_2 doped AlGaAs
171	5.0 × 10^{10}	O_2 doped AlGaAs
209	5.0 × 10^{10}	Undoped AlGaAs
211	1.0 × 10^{10}	H_2 doped AlGaAs
212	5.0 × 10^{10}	O_2 doped AlGaAs
213	1.0 × 10^{10}	O_2 doped AlGaAs

3.7 Transistor Test Structure

Rockwell International Electronics Research Center, Thousand Oaks, has long been involved in the fabrication and characterization of GaAs microwave transistors.[13] Progress in this technology has produced a well established one micrometer gate length device. This transistor structure was used to gather preliminary device results on MBE layers grown in this program.

SHEET RESISTANCE

Al = 7%

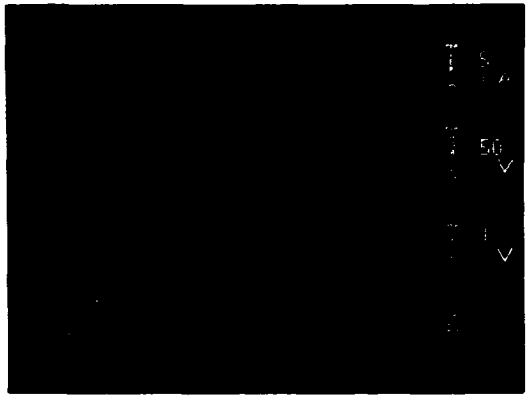

Al = 15%

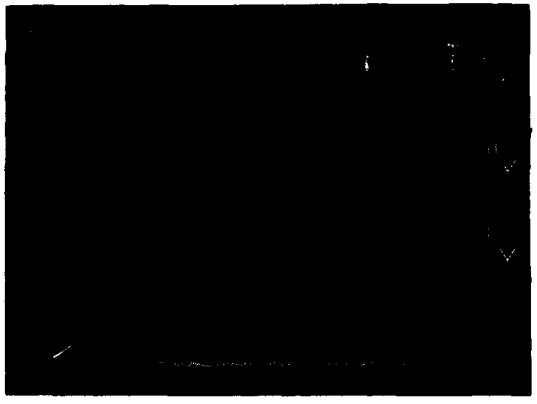

AMBIENT LIGHT
Au-Ge-Pt CONTACTS
$C(0) < 0.1$ pF, 5×10^{-4} cm^2
$C/A \sim 60$ pF/cm^2

Fig. 3.10 I-V characteristics of high resistivity AlGaAs.

These devices are depletion mode field effect transistors fabricated in a mesa format. The gate length is nominally 1 μm and the gate width is 300 μm. The gate is situated 0.25 μm closer to the source than to the drain within a drain-to-source gap of 3 μm. All pattern definition, including the gate, is achieved by the use of conventional photolithographic techniques. The gate metalization system is a Ti/Pt/Au combination, chosen to provide high reliability, having a total thickness of approximately 0.5 μm. Our experience has shown that this metal system is much less prone to burn out than Al gates. The ohmic contact system is an Au-Ge eutectic layer covered with a thin layer of Pt and alloyed at 450°C.

The device chips are mounted in 70 mil ceramic-gold packages for applications up to 10 Ghz. For frequencies at or above 10 GHz, the device chips are generally mounted upon a simple disk carrier which features very low parasitic capacitances in the drain and gate connections.

4.0 SUMMARY

4.1 SIMS Profiles of GaAs/AlGaAs Structures

Multilayer test structures of doped GaAs on AlGaAs were analyzed using SIMS. Atomic constituent profiles of the interface between the GaAs and AlGaAs layers were abrupt. This is an expected characteristic of the MBE growth technology.

The sensitivity in present CAMECA spectrometers provides the measurement of impurity concentration down to 10^{15} cm^{-3} for most elements excluding O_2. Improvements are being sought, with the use of cryogenic pumping, to reduce background levels below their present value.

4.2 PITS Measurements of MBE GaAs/AlGaAs Layers

Photo-induced current transient spectroscopy has provided a new level of sensitivity and resolution for trap detection and characterization in both semi-insulating and conductive samples. The PITS technique was used to analyze MBE AlGaAs samples grown for this program and was found to be successful in identifying trapping centers which were not readily observable by other techniques. Improvements in PITS theory is being pursued for wide band gap materials which will allow this technique to become a very useful analytical tool.

4.3 H_2 and O_2 Doping Experiments

Initial experiments with H_2 additions did not show any reduction in either shallow or deep level incorporation; further work with hydrogen will be resumed after the next system clean up where background impurity concentrations would be lower.

The use of O_2 as a deep compensating impurity was effective and could be used up to 1×10^{-6} torr without introducing microstructural defects. The impurity profiles produced by MBE GaAs-AlGaAs(O)-GaAs (subst) were abrupt and well ordered. The intrinsic MBE AlGaAs layers were already semi-insulating and no further increase in sheet resistance was observed by O_2 doping. Fur-

ther measurement of deep traps related to O_2 by PITS will be of interest in determining the O_2 incorporation in these layers.

4.4 Evaluation of GaAs/AlGaAs Structures

GaAs active layers were grown in situ on semi-insulating AlGaAs/GaAs structures. C-V impurity profiles were used to evaluate active layer doping density vs depth for these structures. Calibration experiments were performed in which a terraced structure with 1000A steps was produced to facilitate the growth of layers with 1-2 $\times 10^{17}$ cm^{-3} carrier concentration and depletion voltage in the 2 volt range for FET device fabrication. Conventional impurity profiles were obtained indicating an abrupt doping profile adjacent to the AlGaAs interface. Some difficulty was experienced with thin active layers which, by growth rate calibration data, should have shown much longer lengths. This apparent "dead layer" effect has been observed in GaAs grown by VPE and LPE methods before and has been attributed to interface states or compensating impurities such as Cr.

5.0 TRANSISTOR RESULTS

5.1 Device Fabrication

Molecular beam epixaxy layers 170 and 210 were used for the fabrication of carrier confinement FETs. The processing steps which have been established for our ion implanted low noise devices were used with the exclusion of the ion implantation preparation. The MBE slices were mesa etched with an ammonium hydroxide-hydrogen peroxide based solution. All of the subsequent metal layers (ohmic, Schottky, overlay) were fabricated by photoresist delineation, metal evaporation deposition and excess metal lifting by photoresist. The ohmic contacts consisted of eutectic Au-Ge with a Pt overlay. This layer was alloyed at 450°C. The Schottky barrier gate metal consisted of Ti/Pt/Au about 0.5 μm total thickness. An overlay metallization of Ti/Au was used to provide the capability of reliably probing and wire bonding to the contact pads.

5.2 Device Characterization

Devices were characterized from MBE layers 170 and 210. These devices, as shown in Fig. 5.1 were tested at wafer level. Because of the low drain currents, observed in Figs. 5.2a and b, these MBE slices were not processed further to enable RF testing. In the light of the satisfactory C-V characteristics of the initial slices and channel current after ohmic contacts, it was concluded that the cause of the low drain current was due to a channel etch before gate metal deposition. The thinning of the channel beneath the gate and the effects of built-in depletion reduced the saturated drain current to that observed in the figures.

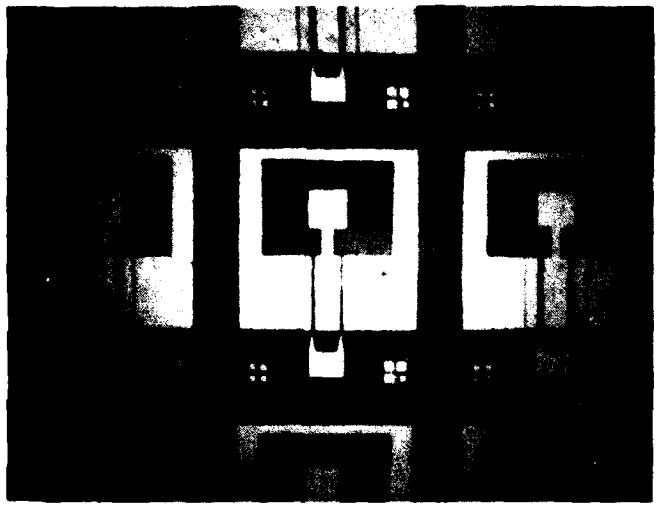

Fig. 5.1 FET devices fabricated from MBE slices 170 and 210.

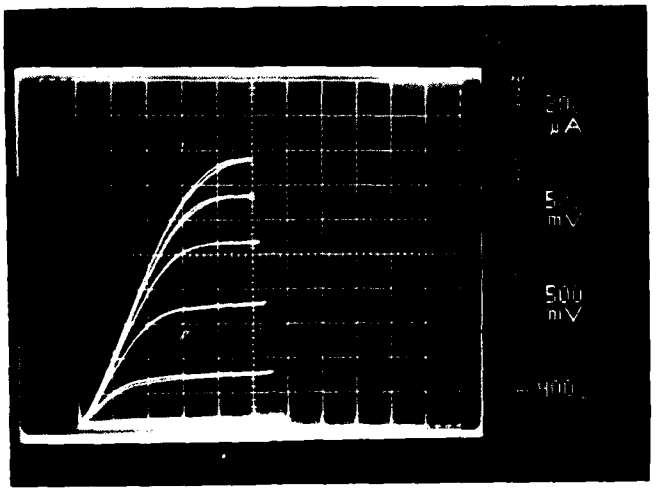

a) MBE 170

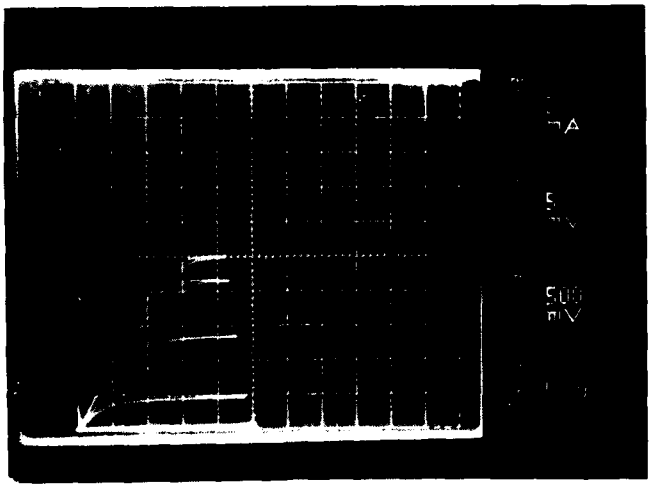

b) MBE 210

Fig. 5.2 FET I-V characteristics of MBE slices 170 and 210.

6.0 CONCLUSIONS

At the present stage of evaluation AlGaAs buffer layers grown by molecular beam epitaxy have shown superior properties over those produced by LPE or VPE methods. During the period 1 May 1978 to 30 April 1979 growths of high purity and intentionally doped AlGaAs MBE have been studied. Characterization of AlGaAs layers grown in this program have shown high resistance properties unavailable from other semi-insulating III-V compounds. Feasibility of producing high quality, semi-insulating AlGaAs has been demonstrated. Active layer structures of GaAs doped with Ge have been grown in situ on AlGaAs buffers that exhibit conventional impurity profiles. Preliminary FET device assessment has shown the need for thicker active layers to permit full rf measurement.

AlGaAs buffer layers have been grown with Al composition between 5 and 100 atomic percent and have shown excellent semi-insulating properties. More definitive materials evaluation will follow through device measurements. Due to the superior semi-insulating properties of MBE AlGaAs conventional Hall and C-V measurements could not be made. High quality semi-insulating GaAs substrates used in these experiments will carry higher shunt current than the AlGaAs layers making mobility and resistivity measurements invalid. Initial measurements of AlGaAs by photo-induced transient current techniques (PITS) have proved quite valuable in assessment of trapping centers in semi-insulating materials. Thermally stimulated current (TSC) was also used to confirm trapping levels observed by PITS measurement. Dark current measurement vs temperautre were used to determine the Fermi level, E_f, and can aid in the interpretation of PITS data.

7.0 FUTURE PLANS

The initial emphasis of the MBE AlGaAs program has been to develop the MBE technology for producing epitaxial buffer layers of AlGaAs as well as active layers of GaAs.

The main thrust of future work in the MBE program will be to fabricate and characterize FET devices. That is, to analyze the electrical properties of MBE material as related to devices as well as to determine the RF performance of low noise field effect transistors fabricated from MBE materials.

The primary test device will be the Rockwell SC-100 low noise FET. This mask set also incorporates a test structure to enable the determination of ohmic contact resistance, C-V and Van der Pauw analysis, and gate resistance measurement. In addition to the low noise FET mask set, an additional mask set is planned which is an array of long gate (fat gate) FETs to allow PITS analysis on a transparent (thin metalization) gate structure.

Because of the layout of the SC-100 mask set, the availability of test structures will allow comprehensive data gathering on the device properties of MBE material. Devices and test structures will also be fabricated on vapor phase epitaxy material of a homostructure nature for direct comparison to the MBE heterostructure material. This will provide valuable information on comparative device performance data, both for DC and RF measurements.

The planned investigation will maintain an effort of fabricating and characterizing devices to determine the guidelines for MBE experiments. Device performance will be the key tool for decisions on the direction of MBE layer growth. Possibilities include the investigation of chrome doping in the growth of the AlGaAs buffer layer, the use of Si doping in the GaAs active layer and AlGaAs as a passivation material on GaAs.

8.0 REFERENCES

1. H. Morkoc, A. Y. Cho, and C. Radice, to be published.

2. A. R. Calawa, Appl. Phys. Lett 33, 1020 (1978).

3. H. C. Casey, Jr., A. Y. Cho, D. V. Lang, and E. H. Nicollian, J. Vac. Sci. Technol. 15, 1408 (1978); H. C. Casey, Jr., A. Y. Cho, and E. H. Nicollian, Appl. Phys. Lett. 32, 678 (1978).

4. D. M. Collins, submitted to Applied Physics Letters.

5. C. Evans & Associates, private communication.

6. Heterostructure Lasers, Part A, H. C. Casey, Jr. and M. B. Panish, Academic Press, 1978, p. 193.

7. F. M. Vorobkalo, K. D. Clinchuk, and V. F. Kovalenko, Sov. Phys. Semicond. 9, 656 (1975).

8. Heterostructure Lasers, Part B, H. C. Casey, Jr. and M. B. Panish, Academic Press, 1978, p. 9.

9. R. D. Fairman, F. J. Morin, J. R. Oliver, Inst. Phys. Conf. Ser. No. 45, 134 (1979).

10. Ch. Hurtes, M. Boulu, A. Mitonneau, and D. Bois, Appl. Phys. Lett. 32, 821 (1978).

11. D. V. Lang, J. Appl. Phys. 45, 3023 (1974).

12. Photoconductivity of Solids, R. H. Bube, John Wiley & Sons, 1960.

13. J. A. Higgins, R. L. Kuvas, F. H. Eisen, and D. R. Ch'en, IEEE Trans. on Elec. Devices ED-15, 587 (June 1978).

DISTRIBUTION LIST - TECHNICAL REPORTS
CONTRACT N00014-78-C-0370

Office of Naval Research (4)
Code 427Y
800 North Quincy Street
Arlington, VA 22217

Naval Research Laboratory
4555 Overlook Avenue, S.W.
Washington, D. C. 20375
Attn: Code 2627 (6)
6810 (1)

Office of Naval Research (1)
Branch Office
1030 East Green Street
Pasadena, CA 91101

Defense Documentation Center (12)
Building 5, Cameron Station
Alexandria, VA 22314

Defense Contract Administration (1)
Services Management Area
Van Nuys - Code S0512A
6230 Van Nuys Blvd.
Van Nuys, CA 91408

Dr. Y. S. Park
AFAL/DHR
Building 450
Wright-Patterson AFB, Ohio 45433

ERADCOM
DELET-M
Fort Monmouth, NJ 07703

Dr. R. Bell, K-101
Varian Associates, Inc.
611 Hansen Way
Palo Alto, CA 94304

Dr. Daniel Ch'en
Rockwell International
Science Center
P.O. Box 1085
Thousand Oaks, CA 91360

Mr. Lothar Wandinger
ECOM/AMSEL/TL/IJ
Forth Monmouth, NJ 07003

Dr. Harry Wieder
Naval Ocean Systems Center
Code 922
171 Catalina Blvd.
San Diego, CA 92152

Dr. William Lindley
MIT
Lincoln Laboratory
F124A, P.O. Box 73
Lexington, MA 02173

Commander
U.S. Army Electronics Command
V. Gelnovatch
(DRSEL-TL-IC)
Fort Monmouth, NJ 07703

Commandant
Marine Corps
Scientific Advisor (Code AX)
Washington, D.C. 20380

Commander, AFAL
AFAL/DHM
Mr. Richard L. Remski
Wright-Patterson AFB, OH 45433

Commander
Harry Diamond Laboratories
Mr. Horst W. A. Gerlach
2800 Powder Mill Road
Adelphia, MD 20783

Advisory Group on Electron Devices
201 Varick Street, 9th Floor
New York, NY 10014

Professor L. Eastman/C. Wood
Phillips Hall
Cornell University
IOthaca, NY 14853

Professors Hauser and Littlejohn
Department of Electrical Engineering
North Carolina State University
Raleigh, NC 27607

Dr. H. Morcog
Coordinated Science Laboratory
University of Illinois
Urbana, Illinois 61801

Professor H. Kroemer
Department of Electrical Engineering
University of California
Santa Barbara, CA 93106